Engineering Structures 257 (2022) 114016

Contents lists available at ScienceDirect

Engineering Structures

journal homepage: www.elsevier.com/locate/engstruct

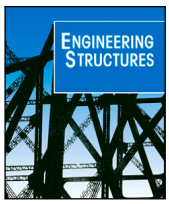

Supervised Deep Learning with Finite Element simulations for damage identification in bridges

Ana Fernandez-Navamuel [a,b,c,*], Diego Zamora-Sánchez [a], Ángel J. Omella [c], David Pardo [c,b,d], David Garcia-Sanchez [a], Filipe Magalhães [e]

[a] TECNALIA, Basque Research and Technology Alliance (BRTA), Parque Científico y Tecnológico de Bizkaia, Astondo bidea, Edificio 700, E- 48160 Derio, Spain
[b] Basque Center for Applied Mathematics (BCAM), Bilbao, Spain
[c] University of the Basque Country (UPV/EHU) Leioa, Spain
[d] Ikerbasque (Basque Foundation for Sciences), Bilbao, Spain
[e] CONSTRUCT-ViBest, Faculty of Engineering, University of Porto (FEUP), Rua Dr. Roberto Frias 4200-465 Porto, Portugal

ARTICLE INFO

Keywords:
Structural Health Monitoring
Deep Learning
Damage identification
Autoencoders

ABSTRACT

This work proposes a supervised Deep Learning approach for damage identification in bridge structures. We employ a hybrid methodology that incorporates Finite Element simulations to enrich the training phase of a Deep Neural Network with synthetic damage scenarios. The neural network is based on autoencoders and its particular architecture allows to activate or deactivate nonlinear connections under need. The methodology intends to contribute to the progress towards the applicability of Structural Health Monitoring practices in full-scale bridge structures. The ultimate goal is to estimate the location and severity of damage from measurements of the dynamic response of the structure. The damages we seek to detect correspond to material degradations that affect wide areas of the structure by reducing its stiffness properties. Our method allows a feasible adaptation to large systems with complex parametrizations and structural particularities. We investigate the performance of the proposed method on two full-scale instrumented bridges, obtaining adequate results for the testing datasets even in presence of measurement uncertainty. Besides, the method successfully predicts the damage condition for two real damage scenarios of increasing severity available in one of the bridges.

1. Introduction

One of the main challenges of Structural Health Monitoring (SHM) in the civil engineering field is the identification and characterization of damage [1,2]. It is an inverse problem that seeks to provide the real health condition of a structure based on experimental measurements [3]. Vibration-based SHM is a widely extended practice that employs the dynamic response of the structure as the damage-sensitive feature [4–6]. It can be addressed through two main approaches, namely, model-based and data-driven [1].

Model-based methods consist of updating the structural properties of a numerical approximation to minimize the discrepancy between its response and that of the real structure [7]. The most widely applied model-based technique in the civil engineering field is Finite Element Model Updating (FEMU) [8]. Some authors, such as Liu et al. [9] and Tran-Ngoc et al. [10], apply it for damage detection in full-scale structural systems. For example, [11] employs a genetic algorithm-based FEMU to a railway bridge with successful location and quantification of damage. But this approach can be time-consuming when a large number of parameters with a wide range of variation are involved [12]. This often prevents its application as a real-time assessment method.

By contrast, data-driven methods rely exclusively on measurements [13]. In recent years, Artificial Intelligence methods, such as Deep Neural Networks (DNNs), have broadened their domain of application to the identification of structural damage [14–16]. These methods undergo a training phase to learn a mathematical relationship between the response of the structure and its health condition [15]. Thus, the computational effort concentrates on the training step, yielding practically real-time predictions. For example, Abdeljaber et al. [17] employ one-dimensional Convolutional Neural Networks (CNN) to detect and locate damage at the different joints of a steel frame in a laboratory environment. An independent CNN is designed and trained for each of the joints. Pathirage et al. [18] propose an autoencoder-based network to identify damage in a small-scale steel frame.

* Corresponding author at: TECNALIA, Basque Research and Technology Alliance (BRTA), Parque Científico y Tecnológico de Bizkaia, Astondo bidea, Edificio 700, E- 48160 Derio, Spain.
E-mail address: afdeznavamuel001@ikasle.ehu.eus (A. Fernandez-Navamuel).

https://doi.org/10.1016/j.engstruct.2022.114016
Received 29 July 2021; Received in revised form 9 January 2022; Accepted 10 February 2022
Available online 7 March 2022

But despite all the improvements achieved in this multidisciplinary practice, SHM-based damage identification is still far from its solid implementation in full-scale civil engineering structures [4,19,20]. Unsupervised approaches are often employed, which only detect departures from a reference (undamaged) condition, but are unable to locate or quantify the damage [21–24]. Some hybrid approaches that incorporate numerical simulations as an additional source of information have been recently investigated [25]. For example, Zhang et al. [26] propose a physics-guided neural network approach to localize damage in structures. They design a loss function that accounts for the discrepancy between the prediction given by the data-driven algorithm and the result of model updating to enhance the diagnostic. Mousavi et al. [27] propose a hybrid technique to detect damage in a laboratory beam structure using a Deep CNN. The network is trained using frequency data from the healthy experimental response and numerical simulations to include damaged scenarios. Authors use the undamaged response to update the parameters of the numerical model before running damage simulations. In [28], authors propose a CNN-based classification approach to identify damage in a pin-joint composite truss structure using synthetic data from FE models. Seventekidis et al. [29] also employ a Convolutional Network classifier to detect structural damage in an experimental benchmark beam. The training phase includes simulated responses from a computational model that is initially updated for the healthy state, including different load conditions and damaged states. However, these works reach only a laboratory level of implementation and their practicality on the full scale has not been demonstrated yet.

This work contributes to the progress towards the practical implementation of SHM-based damage identification techniques for bridge structures [4]. The scarcity of experimental data (mainly of damaged scenarios) together with limited availability of computational resources often prevents an exact location and quantification of damage [12,30]. We propose a combined SHM methodology to complement more exhaustive inspections (e.g. non-destructive tests) for damage identification. These practices can be extremely inefficient (and costly) if no prior knowledge exists to orientate the search [4].

Our goal is to detect the presence of damages that result in a loss of stiffness at some extended part of the structure. Particularly, the damages that we attempt to detect correspond to material degradations that affect a wide area of the bridge. Other damages such as emerging cracks, fatigue, and deformations at various points of the structure [31], are out of the scope of this work. In concrete structures, examples of the sought damages are undermined foundations, eroded piles, abrasion of deck surfaces, etc [32]. They may occur due to the effect of particular operating conditions, such as extreme temperature levels, rise in water flow, and highly humid ambient [33]. We assume these damages affect the bending stiffness properties at the damage location, which yields changes in the dynamic response of the bridge structure [34]. Recognizing the damage type is out of our identification scope. Instead, we expect to infer which part of the bridge has undergone damage and estimate its degree of severity. This is an insightful outcome to enhance the execution of further explorations that would become impractical otherwise.

The proposed method is similar to those presented by Mousavi et al. [27] and Seventekidis et al. [29] in the sense that they address hybrid approaches, but they remain in a laboratory domain. Here, we design the methodology focusing on its application to large systems with complex parametrizations and structural particularities. Compared to [27,29], which employ classification methods, we propose a regression approach to predict location and severity of damage as continuous variables, yielding a more realistic and easily interpretable output.

Given the shortage of experimental measurements and their limitation to the undamaged state, we endow the training phase with massive simulations from a parametrization of the structure using Finite Element (FE) models. This incorporates structural knowledge to the data-driven approach and broadens the solution space with the inclusion of damaged scenarios [26]. To obtain meaningful results, we first update the values of a parametrization of the structure for the healthy condition. We address this step using measurements from a short-term ambient vibration test. The updating helps to attain more accurate numerical responses as it reduces model uncertainty [35].

The data-driven technique seeks to establish a relationship between the dynamic response and the health condition of the bridge. We propose a particular neural network based on autoencoders [36]. Traditional autoencoders perform an encoding step to compress the input data and a subsequent decompression (decoding) to recover most of the original information [37]. Here, we build a two-module architecture analogous to an autoencoder. The first module corresponds to the encoding step and compresses the input data into a lower-dimensional representation. Instead of decoding, the second module learns a mapping from the compressed input into the damage characteristics, namely, location and severity. The main particularity of the network architecture lies in the composition of both modules. We divide each module into two adding terms: a linear and a nonlinear one. The linear term consists of a single layer affine transformation. The nonlinear term incorporates the nonlinearity to the network and follows a feed-forward topology [38]. This architecture enables us to work with a simpler and explainable [39] architecture in cases where nonlinearities have a small contribution.

Pathirage et al. [18] also used autoencoders to identify damage in a small-scale frame structure. They employed the stiffness reduction (due to damage) at each element of the system directly as the output variables to be predicted. However, this approach may become unfeasible for full-scale bridge structures, where several properties of different types are involved. In this work, we propose a more manageable solution with only two output variables: location and severity. We attain this by dividing the structure into sub-regions (locations) where we want to locate damage. We then establish a relationship between the changes in stiffness properties at each location and the severity level. This approach allows easily adapting different models (finer parametrizations, complex structural components, etc.) without penalizing the prediction efficiency of the network. This adaptation ability is one of the contributions of the present work.

We first validate the method in a full-scale concrete structure in Porto. It is the Infante Dom Henrique Bridge [40], a singular deck-stiffened arch bridge with a prestressed reinforced concrete box beam. We investigate the robustness of the methodology by including measurement noise and environmental variability as an adding term to the outcomes of the numerical simulations. Results demonstrate that the neural network delivers adequate predictions even in the presence of measurement error. The unavailability of real data coming from unhealthy scenarios forces to validate the method using synthetic unseen damage cases previously defined by Magalhães et al. [40]

To demonstrate the adaptability of the method, we apply it to another very different structure: the Z24 bridge, in Switzerland [41]. This is a benchmark case study in the scientific community that allows testing the methodology using experimental measurements from damaged scenarios. Here, we successfully detect a pier settlement of increasing depth (40 mm and 80 mm).

2. Methodology

2.1. Problem description

In this work, we propose a supervised learning approach for damage identification in bridge structures. Let B be the bridge under consideration. We denote by $\mathcal{F}$ to the operator that solves the partial differential equations governing the structural behavior of B and subsequently calculates its dynamic response:

$$\mathbf{R}_B = \mathcal{F}(B), \tag{1}$$

with $\mathbf{R}_B = \{\mathbf{f}_B, \boldsymbol{\phi}_B\}$. Here, $\mathbf{f}_B \in \mathbb{R}^{n_m}$ includes n_m eigenfrequencies and $\boldsymbol{\phi}_B \in \mathbb{R}^{n_o} \times \mathbb{R}^{n_m}$ contains the corresponding n_o-dimensional eigenmodes.

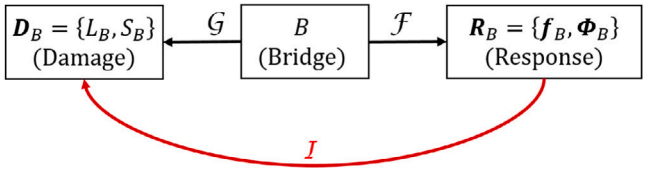

Fig. 1. Block diagram of our SHM problem.

The presence of damage affects the structural properties in B. We denote by $\mathcal{G}$ to the operator that produces the damage characteristics from the bridge condition: $\mathbf{D} = \{L_B, S_B\} = \mathcal{G}(B)$. Here, $L_B \in [1, 2, \dots, n_z]$ indicates the location of damage among n_z zones in the bridge. Depending on the bridge type, these zones can be portions of the spans along the deck, or refer to elements with a particular structural function, such as regions near piers or abutments. The damage severity $S_B \in [s_{min}, s_{max}]$ indicates the extent of damage. Damages below s_{min} are considered negligible and damages above s_{max} are unlikely to occur before an action is taken. The damage identification problem consists of finding the characteristics of damage from measurements of the dynamic response of the bridge:

$$\mathbf{D}_B = \mathcal{I}(\mathbf{R}_B), \tag{2}$$

where $\mathcal{I}$ is the inverse operator. Fig. 1 shows a diagram of the problem, where the inverse operation of damage characterization is highlighted in red.

The methodology is structured as follows: (i) we build a computational parametrization to approximate B; (ii) we update the values of the parametrization to match a measured response during normal operation; (iii) we establish a relationship between the parametrization values and the characteristics of damage; (iv) we generate a database of damage scenarios with different locations and severity levels; finally, (v) we build a DNN to approximate $\mathcal{I}$ with small error and predict damage in B from dynamic data.

2.2. Parametrization of the bridge

Let $B_\theta = \{\theta_1, \dots, \theta_{n_z}\}$ be a parametrization that represents B with n_z different zones. The number of zones to locate damage depends on the density of sensors in the monitoring system. The parametrization includes elastic material properties, cross-section areas, and spring stiffness constants to describe boundary conditions. Each zone in B_θ is described by a subset of properties $\boldsymbol{\theta}_i = \{\theta_1, \dots, \theta_{n_{\theta_i}}\}$. A Finite Element solver $\mathcal{F}^{FE}$ is employed to produce the dynamic response of the parametrization B_θ:

$$\mathbf{R}_{B_\theta} = \mathcal{F}^{FE}(B_\theta). \tag{3}$$

Here, $\mathbf{R}_{B_\theta} = \{\mathbf{f}_{B_\theta}, \boldsymbol{\phi}_{B_\theta}\}$ contains the eigenfrequencies and eigenmodes of the parametrization. For simplicity in notation, we refer to $\mathcal{F}^{FE}$ as $\mathcal{F}$ since the difference between both operators is considered to be negligible.

2.3. Update the values of the parametrization for the healthy state

Under normal operating conditions, the bridge B_u is assumed to be undamaged with a dynamic response $\mathbf{R}_{B_u} = \{\mathbf{f}_{B_u}, \boldsymbol{\phi}_{B_u}\}$. In large-scale structures, $\mathbf{R}_{B_u}$ is often measured through a short-term ambient vibration test and subsequently, the dynamic properties are obtained using Operational Modal Analysis (OMA) techniques [42,43]. This approach is deterministic and lacks consideration of environmental and operational variability. When more measurements are available, a more complete characterization of the healthy state is achieved using for example bayesian techniques [44].

The initial parametrization values are set to $B_\theta = B_{\theta_0}$ based on design properties and engineering knowledge. This yields the preliminary numerical response as $\mathcal{F}(B_{\theta_0})$. However, the real material properties (e.g., the elastic modulus of concrete or steel) in B are uncertain, and modeling boundary conditions (such as piers or abutments) implies assumptions and simplifications. This makes the preliminary solution differ from $\mathbf{R}_{B_u}$.

The goal of the updating step is to obtain a solution B^*_θ that makes $\mathbf{R}_{B^*_\theta}$ approximate $\mathbf{R}_{B_u}$ with small error. This inverse problem is formulated as the minimization of the discrepancy between the numerical and the experimental responses in the l_2 norm:

$$B^*_\theta := \arg\min_{B_\theta} \|\mathcal{F}(B_\theta) - \mathbf{R}_{B_u}\|_2. \tag{4}$$

The variation intervals of the parameters contained in B_θ must ensure consistency in the structural sense to represent a healthy condition. Hence, $B^*_\theta = \{\theta^*_1, \theta^*_2, \dots, \theta^*_{n_z}\}$ yields the values of material properties and boundary conditions that adequately represent the undamaged state of B.

2.4. Damage characterization

In this step, the relationship $\mathcal{G}$ between the structural properties of the bridge B_θ and the damage characteristics $\mathbf{D}_{B_\theta} = \{L_{B_\theta}, S_{B_\theta}\}$ is established. It is assumed that only one of the n_z zones experiments damage at a given time. Thus, when damage occurs at the ith zone, the location is given by $L_{B_\theta} = i$.

Damage severity in B_θ is defined as

$$S_{B_\theta} = \mathcal{G}(\boldsymbol{\theta}_i) = \sqrt{\frac{1}{n_{\theta_i}} \sum_{j=1}^{n_{\theta_i}} {s_{i,j}}^2}, \tag{5}$$

where $s_{i,j}$ are the individual severity values for each involved property, described next. The reduction vector $\boldsymbol{\alpha}_i \in [\mathbf{l}_i, 1]^{n_{\theta_i}}$ affects the structural properties such that $\boldsymbol{\theta}^d_i = \boldsymbol{\alpha}_i \boldsymbol{\theta}^*_i$. The lower bounds $\mathbf{l}_i \in \mathbb{R}^{n_{\theta_i}}$ contain the maximum admissible reduction value for each property in $\boldsymbol{\theta}_i$ based on engineering knowledge to ensure structural sense. The remaining subsets of properties $\boldsymbol{\theta}_j$ $(j \neq i)$ keep their undamaged value in B^*_θ. Thus, the parametrization for a certain damage scenario at the ith zone is $B^d_\theta = \{\boldsymbol{\theta}^*_1, \dots, \boldsymbol{\theta}^d_i, \dots, \boldsymbol{\theta}^*_{n_z}\}$.

The relationship between severity and reduction factor depends on the type of structural property, which can be material or section properties (type a), and/or boundary conditions (type b). This is needed due to the different sensitivity of the dynamic response to property changes from these two groups. For type a, the value of the reduction factor is directly obtained as:

$$s_{i,j} = 1 - \alpha_{i,j} \qquad j = 1, \dots, n^a_{\theta_i}, \tag{6}$$

where $n^a_{\theta_i}$ is the number of a type properties at the ith location. For type b, a different scale is employed to induce effective damage in the structure. In this case, the relationship between the reduction factor and its corresponding severity level is:

$$s_{i,j} = \frac{s_{max}}{\log_{10}(l_{i,j})} \log_{10}(\alpha_{i,j}) \qquad j = 1, \dots, n^b_{\theta_i}, \tag{7}$$

with $n^b_{\theta_i} = n_{\theta_i} - n^a_{\theta_i}$ and $l_{i,j}$ being the jth element in the lower bound vector $\mathbf{l}_i$.

2.5. Database generation

A database is generated that contains damage scenarios of different severity at each location. While location is a discrete variable that takes values between 1 and n_z, severity is a continuous variable. To uniformly sweep the severity interval, we build an iterative process to create different scenarios.

For each sample at the ith zone, an initial sampling generates the value of S_{B_θ} from a uniform distribution: $S_{B_\theta} \sim U(s_{min}, s_{max})$. This is the target value to achieve with the individual severity values of each

Algorithm 1: Generation of damaged scenarios with uniform severity

Input: θ^*, s_{min}, s_{max}, $\boldsymbol{l}_i$, n_{θ_i}, a, b
Output: B_θ^d, S_{B_θ}
/* */
/* Part I: Initialization */
$S_{B_\theta} \leftarrow rand(\mathcal{U}(s_{min}, s_{max}))$; // Obtain posterior severity value
$B_\theta^d \leftarrow B_\theta^*$; // Initialize the damaged parametrization
$\alpha_{i,j} \leftarrow 0, \quad j = 1, ..., n_{\theta_i}$; // Initialize reduction vector $\boldsymbol{\alpha}_i$
/* */
/* Part II: Obtain a damaged parametrization θ^d */
while *any* $(\alpha_{i,j} < l_{i,j} \quad or \quad \alpha_{i,j} > 1 \quad j = 1, ..., n_{\theta_i})$ **do**
  for $j \leftarrow 1$ **to** n_{θ_i} **by** 1 **do**
    $\bar{s}_{i,j} \leftarrow rand(\mathcal{U}(0, s_{max}))$; // Obtain the preliminary individual severity values $\bar{\mathbf{s}}_i$
  Obtain $\bar{S}$ from Eq. (5). ; // Calculate the preliminary severity $\bar{S}$
  Obtain $\mathbf{s}_i$ from Eq. (8); // Obtain the severity values
  /* Calculate the reduction vector $\boldsymbol{\alpha}_i$ */
  for $j \leftarrow 1$ **to** n_{θ_i} **by** 1 **do**
    if *property type* $= a$ **then**
      Calculate $\alpha_{i,j}$ from Eq. (6)
    if *property type* $= b$ **then**
      Calculate $\alpha_{i,j}$ from Eq. (7)
/* Part III: Obtain the damaged bridge B_θ^d */
$\theta_i^d \leftarrow \boldsymbol{\alpha}_i \theta_i^*$; // Calculate the subset of damaged properties θ_i^d
$B_\theta^d \leftarrow \{\theta_1^*, ..., \theta_i^d, ..., \theta_{n_z}^*\}$; // Build the damaged bridge parametrization
Return $\{B_\theta^d, S_{B_\theta}\}$

property at the damaged location using Eq. (5). Random values are first generated for the individual severity of each property as: $\bar{s}_{i,j} = rand(U(0, s_{max}))$, with $j = 1, \dots, n_{\theta_i}$. The severity level $\bar{S}$ is calculated by replacing $\bar{s}_{i,j}$ in Eq. (5). The individual severity value is then corrected to produce S, using the following expression:

$$\mathbf{s}_i = \frac{S}{\bar{S}} \bar{\mathbf{s}}_i \tag{8}$$

The reduction vector $\boldsymbol{\alpha}_i$ is subsequently obtained from Eqs. (6) and (7). If any element in $\boldsymbol{\alpha}_i$ lies out of the admissible interval $[\mathbf{l}_i, 1)$, a new random set of individual severity values $bar\mathbf{s}_i$ is generated and $\boldsymbol{\alpha}_i$ is re-calculated. This step is repeated iteratively until a correct set of reduction factors is achieved. The damaged properties are finally obtained as $\theta_i^d = \boldsymbol{\alpha}_i \theta_i^*$. The damaged bridge is given by $B_\theta^d = \{\theta_1^*, \dots., \theta_i^d, \dots, \theta_{n_z}^*\}$. Algorithm 1 describes this iterative procedure to obtain valid damage scenarios with uniformly distributed severity ($L_{B_\theta} = i$).

Algorithm 1 is applied to obtain n damage scenarios for each structural region $i = 1, \dots, n_z$. This results in $N = n_z \times n$ samples conforming the database. The corresponding dynamic responses are calculated by solving:

$$\mathbf{R}_{B_\theta}^{(k)} = \mathcal{T}\left(B_\theta^{d_k}\right) \qquad k = 1, \dots, N \tag{9}$$

The kth sample in the database contains the dynamic response $\mathbf{R}_{B_\theta}^{(k)} = \{\mathbf{f}_{B_\theta}^{(k)}, \boldsymbol{\phi}_{B_\theta}^{(k)}\}$ and the corresponding damage condition of the bridge $\mathbf{D}_{B_\theta}^{(k)} = \{L_{B_\theta}^{(k)}, S_{B_\theta}^{(k)}\}$.

2.6. Deep neural network

The final goal of the proposed methodology is to identify the damage state of the bridge from measurements of its dynamic response. The operator $\mathcal{I}$ (see Fig. 1) introduced in Section 2.1 establishes the relationship between the dynamic response $\mathbf{R}_B$ (input) and the damage characteristics $\mathbf{D}_B$ (output). The dimension of the input layer depends on the number of mode shapes (n_m) and available measurement points or sensors (n_0) that describe the dynamic response of the bridge, being: $m = n_m(n_o+1)$. Let $\mathcal{I}_\gamma$ be a DNN that approximates the inverse operation of damage identification $\mathcal{I}$:

$$\mathbf{D} \approx \mathcal{I}_\gamma(\mathbf{R}_{B_\theta}; \boldsymbol{\gamma}), \tag{10}$$

where $\boldsymbol{\gamma}$ includes the parameters of the DNN.

Step 1: Pre-processing:
Due to the disparity between the two output variables (location and damage severity) in $\mathbf{D}$, a linear rescaling into the interval $[0.5, 1.5]$ is applied. This interval is selected as it is of unit length and ensures correspondence between relative and absolute errors [45]. For a certain variable $\mathbf{x}$, let $x_{min} := min(\mathbf{x})$ and $x_{max} := max(\mathbf{x})$. The rescaling function $\mathcal{R}$ is defined as:

$$\mathcal{R}(\mathbf{x}) = \frac{\mathbf{x} - x_{min}}{x_{max} - x_{min}} + 0.5 \tag{11}$$

Thus, the rescaled damage condition is obtained as $\mathbf{D}_{resc} = \mathcal{R}(\mathbf{D})$. For simplicity in notation, in the following, the rescaled health condition $\mathbf{D}_{resc}$ is referred to as $\mathbf{D}$.

Step 2: Loss function: The discrepancy between the predicted damage condition $\mathcal{I}_\gamma(\mathbf{R}_B)$ and the real state $\mathbf{D}_B$ is measured employing the l_2 norm of the following loss function:

$$\mathcal{L}_\gamma = \|\mathcal{I}_\gamma(\mathbf{R}_B) - \mathbf{D}_B\|_2 \tag{12}$$

Step 3: Network architecture: A particular NN architecture based on autoencoders [36] is proposed in this work. Autoencoders perform an encoding step to compress the input into a lower-dimensional vector and subsequently decompress it (decoding step) to recover most of the original information [37]. Here, we rely on autoencoder approaches but substitute the decoding step by a mapping between the encoded input and the structural damage (location and severity).

The architecture contains two connected modules. The first module solves the encoding task of data compression. The second module finds a relationship between the compressed input and the damage characteristics. Each module is created by adding a linear and a nonlinear term. With this architecture, when the addressed problem is straightforward and nonlinearities have a small contribution, the nonlinear terms can be deactivated. Fig. 2 describes our proposed network topology.

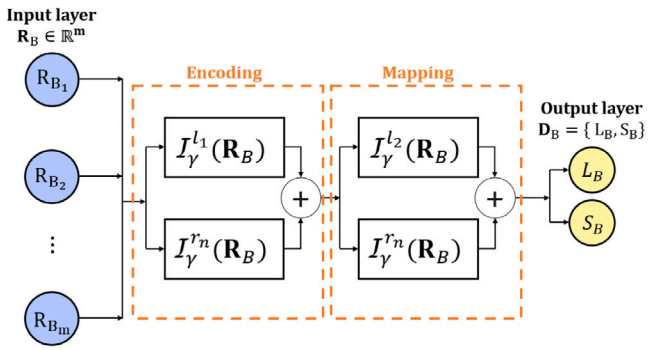

Fig. 2. Block diagram of our proposed Neural Network.

For the first module, we have: $\mathcal{I}_\gamma^1 = \mathcal{I}_\gamma^{l_1} + \mathcal{I}_\gamma^{n_1}$. The linear branch $\mathcal{I}_\gamma^{l_1}(\mathbf{R}_B;\boldsymbol{\gamma}_{l_1})$ applies an affine transformation to the input layer through one single dense layer. This transformation is analogous to Principal Component Analysis (PCA), one of the most traditional data compression techniques [46]. $\boldsymbol{\gamma}_{l_1}$ contains the weights and bias parameters of the operation. The nonlinear branch $\mathcal{I}_\gamma^{n_1}(\mathbf{R_B};\boldsymbol{\gamma}_{n_1})$ undergoes a feed-forward architecture [38] that applies a linear transformation followed by a nonlinear activation function g through L_{n_1} layers. The parameter vector $\boldsymbol{\gamma}_{n_1}$ includes the weights and bias of the operation. The output of the first module enters a second module with analogous architecture that performs the feature mapping.

The output layer adds the linear and the nonlinear connections of the second module: $\mathcal{I}_\gamma^{l_2}(\mathcal{I}_\gamma^1;\boldsymbol{\gamma}_{l_2}) + \mathcal{I}_\gamma^{n_2}(\mathcal{I}_\gamma^1;\boldsymbol{\gamma}_{n_2})$. This layer is customized to restrict the output variables to the admissible rescaled interval. Let C be the clipping function into the interval $[0.5, 1.5]$:

$$C(x;0.5,1.5) = \begin{cases} 0.5 & if \quad x < 0.5 \\ x & if \quad 0.5 \le x \le 1.5 \\ 1.5 & if \quad x > 1.5 \end{cases} \tag{13}$$

The last step is to undo the rescaling operation in Eq. (11) to obtain the real values of the output variables.

Step 4: Training: The database generated in Section 2.5 is employed to train the DNN ($\mathcal{I}_\gamma$) and obtain the set of optimal parameters $\boldsymbol{\gamma}^*$ that produces an approximation to $\mathcal{I}$. This yields:

$$\boldsymbol{\gamma}^* := \arg\min_{\boldsymbol{\gamma}}(\mathcal{L}_\gamma) \tag{14}$$

Here, an stochastic gradient descent method is employed to solve the minimization problem [38]. Tensorflow library available in Python environment is used to carry out the whole process [47].

The final goal is to employ the DNN to make predictions on new measured data from the monitoring systems operating in bridge structures. Fig. 3 shows a flowchart of the whole procedure. We can divide the different tasks into offline and online. The offline part includes all the required steps to build the damage identification system. The online part consists of acquiring new measurements from the bridge to feed the DNN and obtain a diagnostic of the health condition.

In this work, we focus on the development of the offline part. The online part consists of the incorporation of the DNN as a real-time assessment tool for SHM. Once new measurements are acquired under an unknown structural condition, the DNN would predict a damage diagnostic. The prediction is to be considered as an assessment that complements visual inspections as well as other SHM systems.

3. Results

In this section, we describe the results obtained for two cases of study. The first one is the Infante Dom Henrique bridge in Porto. This bridge is currently under service and is being monitored. However, data regarding real damage scenarios is unavailable. We subsequently apply the proposed method to the Z24 bridge in Switzerland. This brings up the opportunity to perform an experimental test. To solve the different tasks, we employed a computer (Dell Precision 3520) with the following specifications: Intel(R) Core i7-7700HQ, 2.80 GHz CPU.

3.1. Case 1: Bridge Infante Dom Henrique

3.1.1. The bridge and monitoring system:

The bridge Infante Dom Henrique bridge (Porto) is a concrete bridge that contains two main interacting elements: a rigid pre-stressed box girder of 4.50 m depth, and a reinforced arch of 1.50 m thickness (see Fig. 4). Due to the high stiffness of the deck compared to that of the arch, the bridge behaves as a beam structure between abutments [48].

The dynamic monitoring system described in this paper was installed and activated in September 2007 and operated for five years. Nowadays, the bridge is being monitored by a simpler wireless monitoring system [49]. Due to existing structural symmetry, only half of the bridge was monitored at four particular sections (see Fig. 5) [48].

The monitoring system included two acquisition modules and 12 uniaxial force balance accelerometers located inside the deck box girder. There are four instrumented sections with three sensors each. For each section, one sensor measures lateral accelerations, and the other two measure vertical accelerations upstream and downstream sides, respectively. Additional information can be found in Magalães et al. [48].

In this work, we focus on the vertical accelerations of the bridge to locate and quantify the damage. Thus, we have access to four vertical acceleration signals (upstream or downstream) from which we calculate the dynamic properties (eigenfrequencies and eigenmodes) using Operational Modal Analysis (OMA) techniques [48]. Fig. 6 shows the first four unity-scaled vertical mode shapes.

While eigenfrequencies are global features, eigenmodes contribute to locating damage. A mode shape describes the level of vibration amplitude for each node of the structure when it is excited with the corresponding eigenfrequency. The presence of damage at a certain location will change differently the mode shape. If changes of the bending stiffness are under investigation, each eigenmode is more sensitive to those damages located close to the regions where the curvature of the mode shape is larger. The number of points describing each eigenmode depends on the number of sensors in the monitoring system. Hence, the monitoring system restricts the zones where damage can be located to those that influence the modal ordinates of the instrumented degrees of freedom. In this work, we restrict the possible damaged regions to the instrumented half of the bridge. Although damages at regions on the left-hand side of the bridge might also be detected, it would be difficult to distinguish their location.

3.1.2. Ambient vibration test

An ambient vibration test is one of the most convenient approaches to estimate the modal parameters of a structure under service [48]. It employs the vibration induced by traffic and wind as the excitation to characterize the response of the structure. The amplitude of the accelerations that the bridge suffers under such excitation is very low. For this reason, especially sensitive sensors must be employed.

In the ambient vibration test carried out at Infante bridge in 2002, four tri-axial 18-bit strong motion recorders were used [48]. All sensors were synchronized through external GPS sensors. During the test, two of the sensors were fixed in the middle-deck cross-section (upstream and downstream) and acted as a reference. The other two sensors changed position within a total of 15 set-ups to cover the length of the bridge deck. For each set-up, records of 16 min were collected with a sampling frequency of 100 Hz. This frequency was reduced to 20 Hz after the application of a low-pass filter. Further details regarding the ambient vibration test can be found in Magalhães et al. [48].

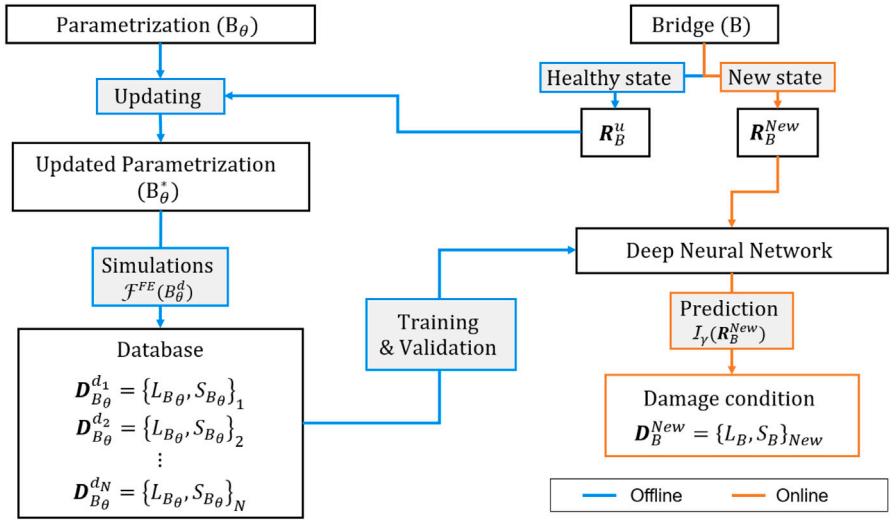

Fig. 3. Flowchart of the proposed methodology.

Fig. 4. Infante bridge view.

3.1.3. Parametrization

We employ a parametrization developed by Magalhães et al. [48]. It includes 3D bar elements in ANSYS® to describe the behavior of the bridge. The structural properties (area, bending and torsion moments of inertia, and shear deflection constants) are included according to design specifications. Since we are investigating the vertical bending response of the structure, 3D bar elements (beam type) have optimal functionality. They also allow introducing damage as a reduction of the corresponding cross-section inertial properties. This type of model was first developed by Magalhães et al. [48] and can be considered an accurate approximation to represent the vertical bending behavior of the bridge. More sophisticated models such as those composed of solid elements could be employed. These provide more precise predictions at the cost of higher computational effort and modeling complexity. But these models can introduce unwanted mode shapes (e.g., vibrations of the cantilever eaves of the deck) and hinder the modal identification process. Besides, the simulation of damage in this type of model may become very complex, since solid elements lack section properties as an accessible parameter. This forces to introduce damage in terms of geometrical variations, which is a non-trivial task that can produce mesh problems and prevents an automatic generation of scenarios.

Magalhães et al. [48] described the calibration process, focusing on the connections of columns and abutments with the deck. While the highest columns (M1 and M6 in Fig. 5) have a monolithic connection, the other columns and abutments contain two unidirectional sliding pot bearings. Three possible connection disposals were considered and analyzed. The authors designed a final parametrization including fixed longitudinal displacement and rotations in the pot bearings at the columns but free at the abutments, and horizontal springs to simulate additional stiffness at the abutments. The value of the stiffness constants in the abutments is fixed manually to approximate the first four vertical bending eigenmodes.

For further steps in this work, we employ the higher-order modes (third and fourth) since they are more sensitive to localized damages such as those sought in this work [50].

According to the position of the sensors, we consider eight possible damage locations along the right-hand side of the bridge, according to Fig. 7. Each location is 17.5 m long along the bridge deck.

3.1.4. Database generation

Given the beam-type behavior of the bridge [48] and the location of the sensors in the monitoring system, we focus on the identification of damages in the deck. Specifically, we employ the real values that describe the cross-section inertia along with the beam-type elements that model the deck. All these structural properties are of type a introduced in Section 2.4. Each location contains 4 properties, resulting in a total of 32 structural properties involved in this case of study. We set the minimum severity to $s_{min} = 2.5\%$ and the maximum to $s_{max} = 50\%$ based on sensitivity analysis and engineering criterion. During sensitivity analysis, we observed that damages below 2.5% barely introduced changes in the response of the structure. The multiplication factors in $\boldsymbol{\alpha}$ range from 0 (undamaged property) to 0.5 (50% damage at that property).

We solve $n = 5{,}000$ damage scenarios for each of the $n_z = 8$ locations, yielding a total of $N = 40{,}000$ samples. The time required to obtain the database was 37.3 h. We calculate the dynamic response for each sample and match it with the corresponding damage label to form the database. Although only four measurement points (sensors) are available in the monitoring system, we obtain seven-dimensional eigenmodes throughout simulations to add extra information for damage location.

We choose some representative samples from the database to study the sensitivity of eigenfrequencies to damage. For each location, we select 10 samples of constant increasing severity from 5% to 50%. Fig. 8 shows the sensitivity of the selected eigenfrequencies.

We observe that the third eigenfrequency is very sensitive to damages at locations L_1 and L_5. This is related to the curvature (change of slope) of the eigenmodes [51]. The higher the curvature of the mode in the affected location, the higher the impact on the corresponding natural frequency [51]. We observe that for location L_3, since it is almost a blind node (small curvature), it barely changes with the

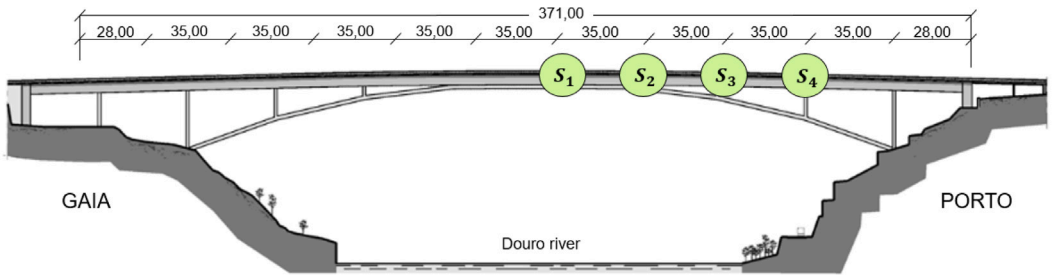

Fig. 5. Instrumented cross-sections in the monitoring system.

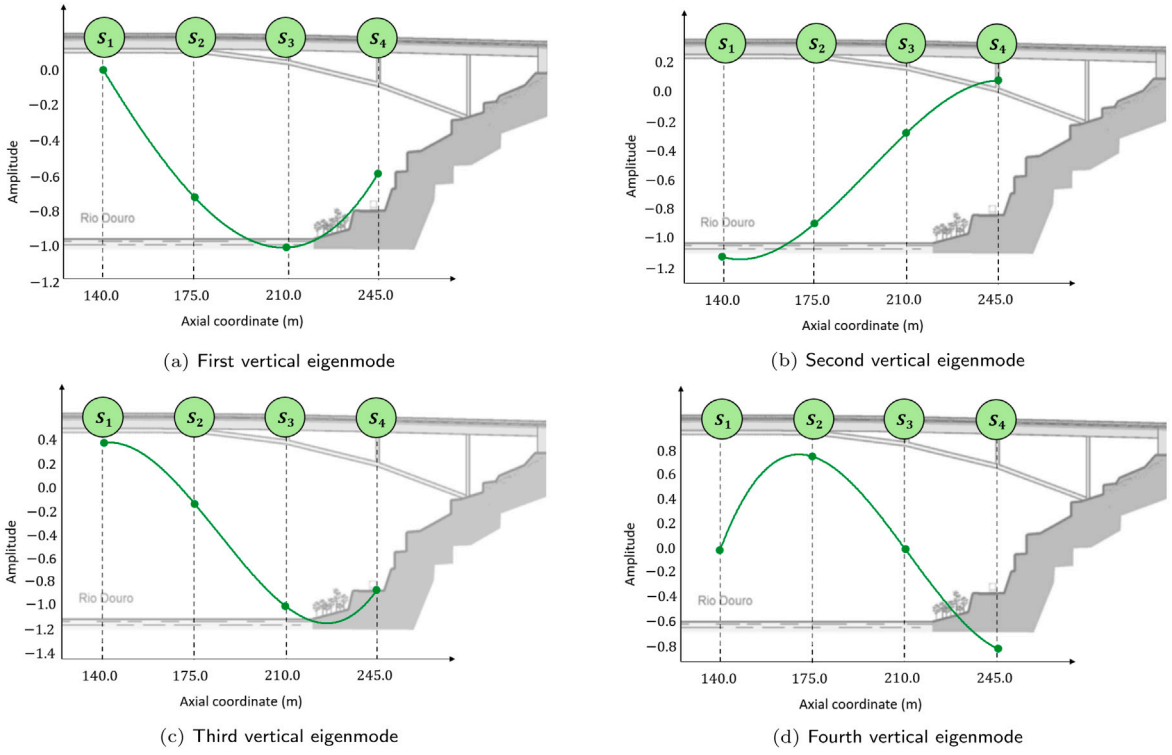

Fig. 6. Vertical eigenmodes obtained from ambient vibration test.

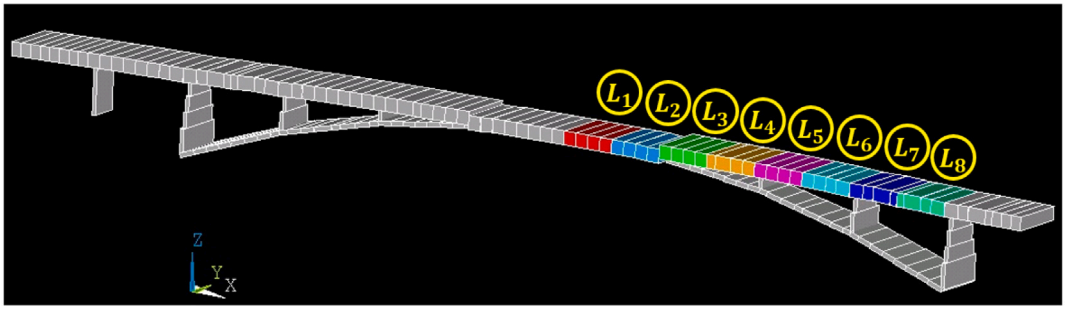

Fig. 7. Parametrization of Infante bridge with eight locations.

increase of severity (see Fig. 6(c)). For the same reason, the fourth vertical eigenfrequency is strongly affected by damages at location L_3 (see Fig. 6(d)).

3.1.5. Deep neural network

We employ the network architecture described in Section 2.6. The nonlinear connections $\mathcal{I}_\gamma^{n_1}$ and $\mathcal{I}_\gamma^{n_2}$ are symmetric and contain four layers each. We employ a "ReLu" [38] activation function at the hidden layers of the nonlinear connection. The input layer receives a total of $m = 16$ input features. These include higher-order (third and fourth) vertical eigenfrequencies and eigenmodes, as indicated in Section 3.1.3. The encoding phase compresses this input into an eight-dimensional feature vector. This topology provides adequate results.

We randomly split the database as follows: 72% of the samples are employed for training, 18% for validation, and the remaining 10% are kept for testing. We train the neural network through 10,000 epochs. This number allows for sufficient training and prevents overfitting. Each epoch constitutes a new passage of the entire training dataset

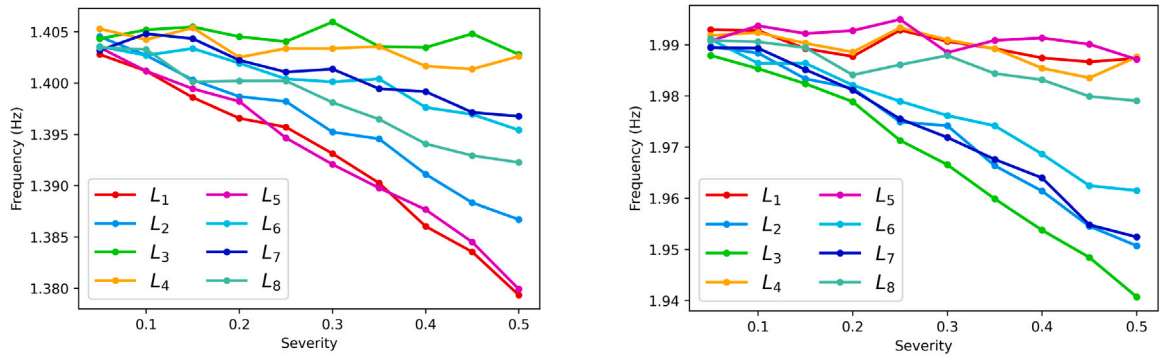

(a) Third vertical eigenfrequency (b) Fourth vertical eigenfrequency

Fig. 8. Evolution of eigenfrequencies with increasing damage severity.

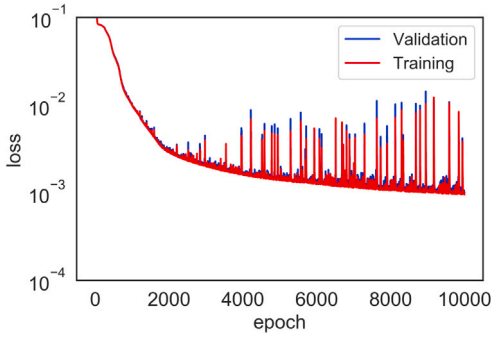

Fig. 9. Loss evolution for the training and validation datasets (Infante bridge).

through the NN [38]. Fig. 9 shows the evolution of the loss function for both the training and validation datasets. The required training time was 12 min. We employ a particular gradient descent optimizer that prevents getting trapped in local minima during training [52]. This optimizer produces high loss function values at certain epochs. To select an adequate solution, we retain the best trained model based on a performance indicator. Here, we select the model that achieves the minimum loss value for the validation dataset.

We evaluate the performance of the trained network for the testing dataset. Fig. 10 includes the cross-plot of the output variables. It exhibits a high correlation between the real value (ground truth) and the prediction given by the DNN. We employ the squared correlation coefficient r^2 as the correlation metric [53]. The distribution of the samples in the graph is represented with a color scale, with a darker color meaning more density of samples.

Fig. 10(a) shows the cross-plot of location for the testing dataset. Although the ground truth is restricted to the eight possible locations, the prediction of the DNN is continuous (regression). Most of the samples concentrate close to the red line (prediction = ground truth), resulting in a high correlation level (r^2). Fig. 10(b) shows the predictions obtained for the severity level. These results show a good performance of the DNN during the numerical test.

Given the lack of real measurements from damage scenarios, we perform a numerical test. We employ two damage cases described by Magalhães et al. [40]. These are considered minor damages according to [40]. They consist in reducing the vertical bending inertia at a small segment of the bridge deck. They were applied at locations L_1 and L_8 according to Fig. 7. We consider two reduction levels – 10% and 30% – for the affected structural property. We estimate the ground truth severity for each scenario according to Eqs. (5) and (6). Table 1 shows the prediction provided by the DNN.

According to Table 1, the DNN is achieving adequate results. However, the lack of experimental damage scenarios prevents a more realistic validation. After training and validation, the algorithm is ready to be implemented in the SHM system. The monitoring sensors will acquire new measurements and produce the current natural frequencies and mode shapes of the structure. To make the experimental eigenmodes (four-dimensional) match the numerical ones (seven-dimensional), we complete them by fitting a spline and obtaining the corresponding value between every two sensors. The completed experimental measurements are fed to the DNN that provides a prediction of the health condition of the structure.

To demonstrate the contribution with respect to other existing techniques, we consider the work developed by Pathirage et al. [18], which also employed an autoencoder trained with numerical simulations to solve the damage identification problem. The main difference lies in the output of the DNN, where for Pathirage et al. [18] is an N-dimensional vector based on the N parameters (structural properties) that can change in presence of damage. N can be considerably large for large-scale structures with complex parametrizations. Besides, this approach requires to adapt the architecture to fit the number of properties of different structures or different parametrizations of the same structure. Our approach applies a post-processing to the structural parameters to make predictions based on a two-dimensional output that describes damage in terms of location and severity. This allows keeping the same architecture (with reduced output dimension) of the DNN regardless of the parametrization and structural system and enhances the interpretation of predictions. Also, the larger is the output (more variables to predict) the more complex gets the training phase and predictions may lose accuracy.

For the case of study of Infante Dom Henrique bridge, the output dimension increases from two to 32 if we employ the approach of Pathirage et al. [18]. We implement this by adapting our DNN to have a 32-dimensional output, where the output corresponds to the reduction vector $\boldsymbol{\alpha}$. Table 2 compares the value of the r^2 metric that measures the correlation between ground truth and prediction of the output variables during testing for both methodologies. The predictions provided by our approach are better than those using the 32-dimensional. Obtaining adequate results using the methodology proposed by Pathirage et al. [18] would require a more complex DNN and a larger training database, which implies more computational effort. Besides, the results provided by our approach are easier to interpret and enhance applicability mainly for complex parametrizations with a large amount of involved structural properties.

3.1.6. Incorporation of measurement uncertainty

In this section, we evaluate the performance of the methodology in presence of measurement noise and environmental variability. A long-term monitoring campaign started in 2007 at Infante bridge that

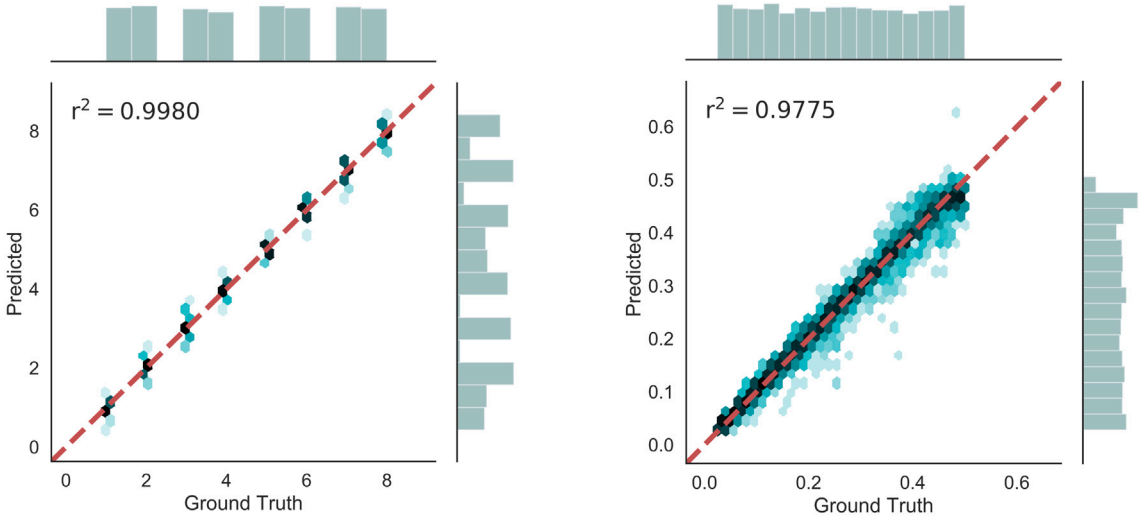

(a) Location cross-plot for the testing dataset

(b) Severity cross-plot for the testing dataset

Fig. 10. Infante bridge cross-plots for the testing dataset. (For interpretation of the references to color in this figure legend, the reader is referred to the web version of this article.)

Table 1
Numerical testing for Infante bridge.

Scenario	Ground truth		Prediction	
	Location	Severity (%)	Location	Severity (%)
10% vertical bending inertia reduction at L_1	1	5.00	1.41	4.21
30% vertical bending inertia reduction at L_1	1	15.00	1.05	13.42
10% vertical bending inertia reduction at L_8	8	5.00	7.89	5.32
30% vertical bending inertia reduction at L_8	8	15.00	8.00	17.85

Table 2
Comparison of metric r^2 value for the output variables during testing using a 2-D approach and a 32-D approach.

Output dimension	Variable								
	Var1	Var2	Var3	Var4	...	Var29	Var30	Var31	Var32
2-D	0.9980	0.9775	–	–	...	–	–	–	–
32-D	0.8591	0.7802	0.7345	0.8371	...	0.6446	0.7531	0.7771	0.8375

contained 12 force balance accelerometers installed in four particular cross-sections of the structure [40,48]. These measurements were subsequently processed to identify the eigenfrequencies and eigenmodes of the bridge.

Some statistical analyses were carried out by Magalhães et al. [48] to explore the variability induced by temperature and other operational phenomena (e.g., concrete hardening) in the eigenfrequencies of the bridge. Table 2 in their work [48] compared the standard deviation (SD) of the first twelve eigenfrequencies for the ambient vibration test and the monitoring campaign, observing much higher values during the monitoring phase due to the effect of temperature. According to their study, any eigenfrequency outranging the interval of its value $+/-1.5$SD could be considered an outlier. This information was unavailable for eigenmodes, while it is known that they are less sensitive to environmental variability [54].

Based on this information, we account for measurement noise and environmental variability as follows: for the eigenfrequencies, we consider the same interval as [48]. To be conservative, we employ the highest SD value amongst the four vertical eigenfrequencies analyzed. For the eigenmodes, we employ the variability observed during the ambient vibration test that includes measurement noise. We incorporate measurement error as an additive term [35] such that:

$$d_{new} = d_{num} + \epsilon, \tag{15}$$

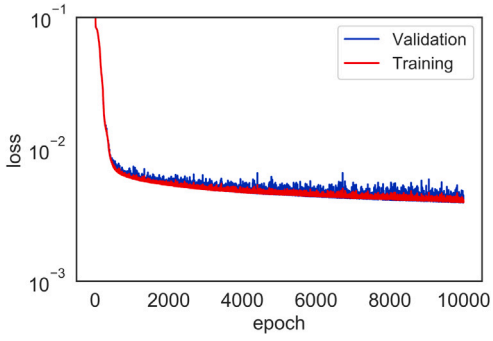

Fig. 11. Loss evolution for the training and validation datasets with measurement uncertainty.

where d_{num} refers to any magnitude obtained from simulations (eigenfrequencies and eigenmode amplitudes), ϵ stands for the additive error term, and d_{new} is the resulting magnitude.

The new database contains three times the original one, including: (i) the original database described in Section 3.1.4, (ii) the original database affected by a reduced error level ($\epsilon \in [-0.0001, +0.0001]$), and (iii) the original database affected by the previously described

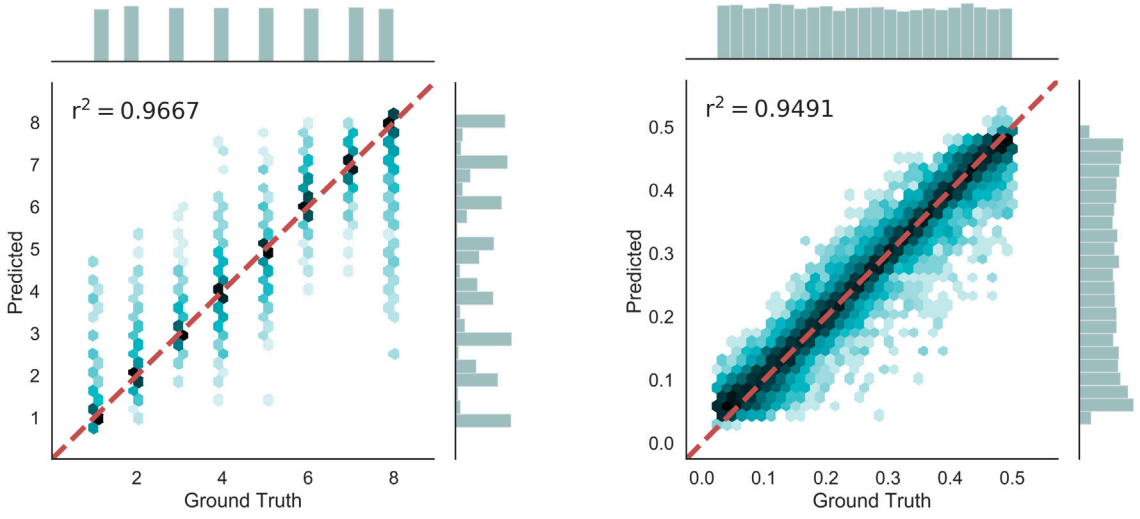

(a) Location cross-plot for the testing dataset

(b) Severity cross-plot for the testing dataset

Fig. 12. Infante bridge cross-plots for the testing dataset with measurement uncertainty.

Table 3
Numerical testing for Infante bridge in presence of measurement uncertainty.

Scenario	Ground truth		Prediction	
	Location	Severity (%)	Location	Severity (%)
10% vertical bending inertia reduction at L_1	1	5.00	1.06	5.93
30% vertical bending inertia reduction at L_1	1	15.00	0.97	15.32
10% vertical bending inertia reduction at L_8	8	5.00	7.83	5.32
30% vertical bending inertia reduction at L_8	8	15.00	8.00	21.36

measurement uncertainty according to [48]. The value of ϵ for each scenario is randomly sampled from the corresponding interval.

We repeat the training and validation process of the neural network for the new database. Fig. 11 shows the loss evolution for the training and validation datasets. The required training time was 28 min.

We then evaluate the performance of the trained network for the testing dataset. Fig. 12 includes the cross-plot of the output variables.

The achieved correlation levels are slightly lower than those obtained in the deterministic approach, but results are still great, demonstrating an adequate performance of the DNN.

Table 3 shows the prediction provided by the DNN for the considered damage scenarios. We observe that the DNN achieves adequate results in predicting both damage scenarios. This example is a preliminary attempt to include measurement error in the process, but more extensive research is required to demonstrate the full capability of the method to operate under diverse noisy and variable environments. We consider this issue as a future research line to explore in forthcoming works.

3.2. Case study 2: Z24 bridge

The Z24 bridge is a post-tensioned concrete two-cell box girder with three spans crossing the highway that connects Bern and Zurich (see Fig. 13). This bridge was demolished in 1998 to expand its span due to an enlargement of the highway [41]. Before demolition, some damage scenarios were generated and monitored during short-term campaigns for different research purposes [55–58]. In this work, we employ two damage scenarios corresponding to a settlement of 40 mm and 80 mm at the Koppigen side pier (see Fig. 13).

3.2.1. Ambient vibration test

Previous to bridge demolition, progressive tests were carried out in the bridge under the SIMCES project, including some damage simulations [59]. Forced and ambient vibration tests were performed for the healthy structure and subsequent damage scenarios. In this work, we employ measurements from the ambient operational vibration tests (11–12 min length records of ambient accelerations including fixed and moving sensors in nine different set-ups) to identify the experimental first and second eigenmodes with high resolution. Further information regarding the configuration and measurements can be found in Reynders et al. [41] The available number of points describing each eigenmode allowed to characterize the dynamic behavior of the bridge with only the first two eigenmodes. We employ the software MACEC [60] to obtain the natural frequencies and mode shapes from the acceleration signals. The first one is a vertical bending, and the second one corresponds to a torsion.

3.2.2. Parametrization

We build a parametrization in ANSYS® using shell elements for the deck and piers and spring type elements to model boundary conditions. The use of shell-type elements is justified here since one of the selected mode shapes to represent the structural behavior corresponds to a torsion. Shell elements provide a better distribution of the structural masses. Other works, such as [61] or [62], propose similar modeling elements, supporting the decision taken and the validity of the model. We consider five different locations (see Fig. 14). The parametrization includes material properties (type *a*) and boundary conditions (type *b*). Material properties refer to the elastic modulus of the concrete. Locations one, two, and three, are described by these properties. Locations one and three include seven material properties, and location two contains 14 along its length. We describe locations four and five (boundary conditions at the piers) with spring constants in the vertical direction (five properties describe each of these locations). A total of 38 properties are involved in this case of study.

We employ a Genetic Algorithm [63] to solve equation (3) and calibrate the parametrization. This yields a good numerical approximation to the response of the real bridge according to the ambient vibration test.

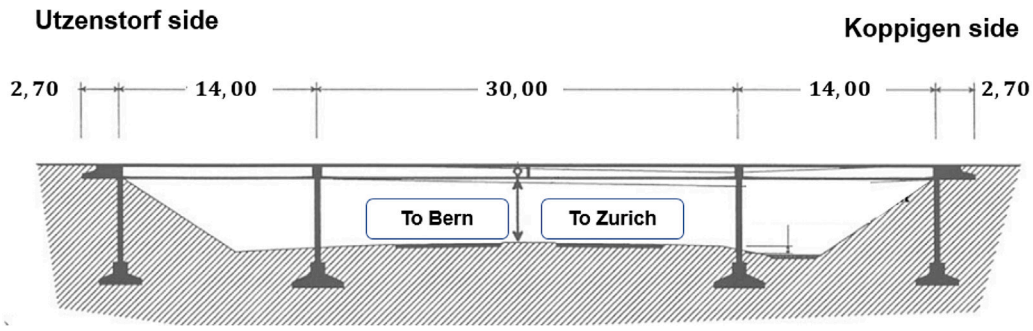

Fig. 13. Z24 bridge in Switzerland [41].

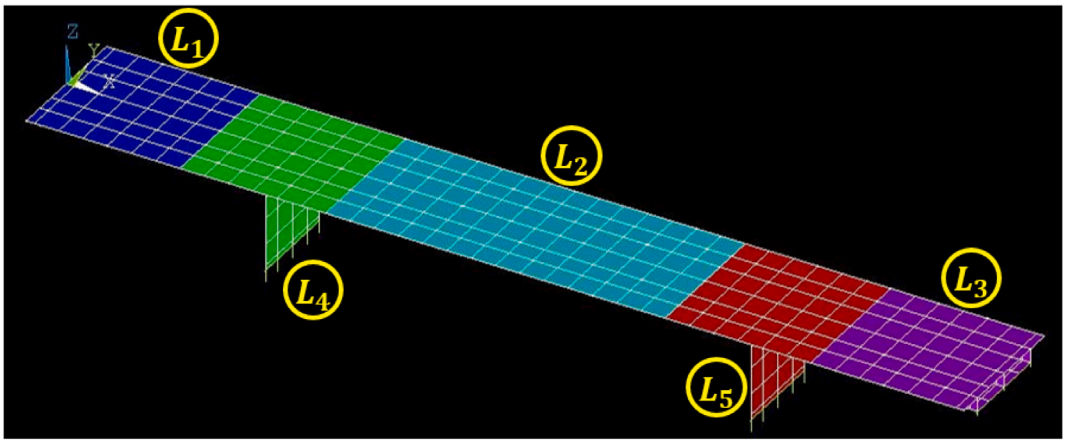

Fig. 14. Parametrization of Z24 bridge with five locations.

Table 4
Results of the updating procedure.

Mode	Initial parametrization		Updated parametrization	
	Freq. error (%)	MAC	Freq. error (%)	MAC
1	0.54	0.9774	0.39	0.9886
2	0.02	0.9871	0.01	0.9930

Table 4 gathers the error terms in frequencies and eigenmodes before and after the updating process. For the eigenmodes, we employ the Modal Assurance Criterion (MAC) values [64].

3.2.3. Database generation

We set the minimum severity to $s_{min} = 0.05$ and the maximum to $s_{max} = 0.5$ based on sensitivity analysis and engineering criterion. During sensitivity analysis, we observed that damages below 5% barely introduced changes in the structural response. The multiplication factors in $\boldsymbol{\alpha}$ range from 0 (undamaged property) to 0.5 (50% damage at that property). We solve $n = 8,000$ damage scenarios for each of the $n_z = 5$ locations, yielding a total of $N = 40{,}000$ samples. The time required to obtain the database was 30.6 h. We calculate the dynamic response for each sample and match it with the corresponding damage label.

3.2.4. Deep neural network

We employ the network architecture described in Section 2.6. The architecture of the neural network contains six hidden layers at the nonlinear connections $\mathcal{I}_\gamma^{n_1}$ and $\mathcal{I}_\gamma^{n_2}$. We employ a "ReLu" [38] activation function at the hidden layers of the nonlinear connection. The input layer receives a total of $m = 46$ input features. These include the first two eigenfrequencies and corresponding eigenmodes. The length of the mode shape vectors is 22 and includes points from both upstream and downstream measurement positions. The encoding phase compresses this input into a 17-dimensional feature vector. This topology provides adequate results.

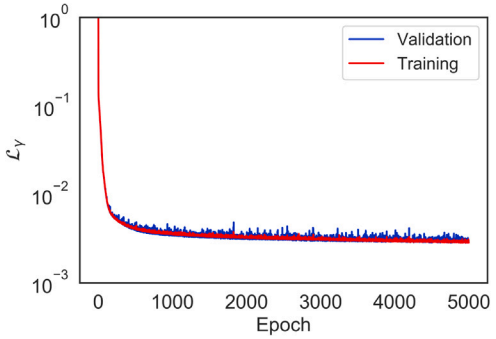

Fig. 15. Loss evolution for the training and validation datasets (Z24 bridge).

We randomly split the database as follows: 72% of the samples are employed for training, 18% for validation, and the remaining 10% are kept for testing. We train the neural network through 5,000 epochs. This number allows for sufficient training while preventing over-fitting. Fig. 15 shows the evolution of the loss function for the training and validation datasets. The required training time was 10 min. We employ an optimizer that prevents from getting trapped in local minima during training [52]. This optimizer produces high loss function values at certain epochs, but we select the model with minimum validation loss.

We evaluate the performance of the trained network for the testing dataset. Fig. 16 includes the cross-plot of the output variables. It shows that a high correlation exists between the real value (ground truth) and the prediction given by the network.

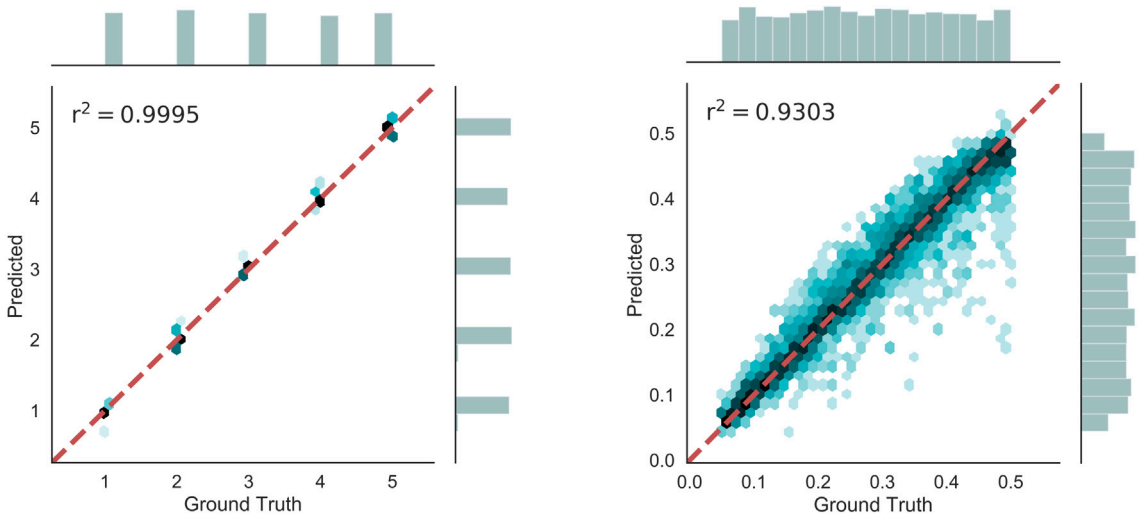

(a) Location cross-plot for the testing dataset.

(b) Severity cross-plot for the testing dataset.

Fig. 16. Z24 bridge testing cross-plots.

Table 5
Experimental validation with two damage scenarios.

Damage	Location	Severity (%)
D1	4.78	30.64
D2	5.00	43.64

Now, we test the network for the available experimental damages. We employ two damages of increasing severity at the pier in the Koppigen side (see Fig. 13), that corresponds to location L_5 according to Fig. 14. The damage consisted of pier settlements of 40 mm (D_1) and 80 mm (D_2) [65]. Both damages are considered to be of high severity [65]. The monitoring datasets consisted of two 10.9 min long time series sampled at 100 Hz. Peeters et al. [66] describe the experiments in more detail. We post-processed the acceleration signals to obtain the responses R^{D_1} and R^{D_2} and evaluated the DNN.

Table 5 gathers the obtained results.

We observe that the DNN correctly predicts the location of the damage. The true severity level is unknown for both scenarios, although we expect to obtain high values that increase from the first scenario to the second one. Accordingly, the obtained results indicate meaningful severity levels (above 30%).

4. Conclusions and future work

We implemented and tested a novel SHM methodology to identify damages that induce stiffness reductions at specific parts of a structure. Experimental measurements from ambient vibration tests were employed to adjust the properties of the parametrization and approximate the real dynamic response (natural frequencies and mode shapes). By grouping the structural properties of the parametrization into various regions where damage may occur, we designed a database that included different scenarios labeled by damage location and severity. The proposed DNN captured the relationship between the dynamic response of the structure and the presence of damage with reduced errors after adequate training. The methodology demonstrated to be easily adaptable to different types of bridges.

We validated the methodology with two full-scale cases of study: Infante Dom Henrique bridge in Porto and Z24 bridge in Switzerland. For the Infante bridge, we obtained adequate results, including successful prediction of two synthetic damage scenarios evaluated as testing. The lack of experimental data prevented a more realistic validation. We also explored the robustness of the method to the presence of measurement error by introducing noise and environmental variability as an adding term to the numerical responses of the database. The availability of two experimental damage scenarios of increasing severity in the Z24 case study allowed us to evaluate the performance beyond the numerical frame. The DNN correctly estimated the location of the pier settlements applied before the bridge demolition. The exact severity level of these damages is unknown, but high values were expected and achieved, demonstrating the ability of the methodology.

We consider as future work the inclusion of environmental and operational variability to allow extending the validity of the approach to different service conditions without the risk of masking the presence of damage. Although in this work we only employed dynamic monitoring data from acceleration signals, in most instrumented bridges different sensor types coexist. These may provide useful information (e.g., temperature, humidity, inclinations, displacements, etc.) to characterize better the healthy state of the bridge. An interesting future study is to consider these variables together with dynamic data as the input for damage detection methods. In this sense, experiences in real bridges such that in the Z24 bridge considered in this work are of huge interest to the research community.

Declaration of competing interest

The authors declare that they have no known competing financial interests or personal relationships that could have appeared to influence the work reported in this paper.

Acknowledgments

This work has received funding from the European's Union Horizon 2020 research and innovation program under the grant agreement No 769373 (FORESEE project). This paper reflects only the author's views. The European Commission and INEA are not responsible for any use that may be made of the information contained therein.

Authors would like to acknowledge the Basque Government funding within the ELKARTEK programme (SIGZE project (KK-2021/00095)).

This work was financially supported by: Base Funding - UIDB/04708/ 2020 of the CONSTRUCT - Instituto de I&D em Estruturas e Construções - funded by national funds through the FCT/MCTES (PIDDAC).

David Pardo has received funding from: the European Union's Horizon 2020 research and innovation program under the Marie Sklodowska-Curie grant agreement No 777778 (MATHROCKS); the European Regional Development Fund (ERDF) through the Interreg V-A Spain-France-Andorra program POCTEFA 2014-2020 Project PIXIL (EFA362/19); the Spanish Ministry of Science and Innovation projects with references PID2019-108111RB-I00 (FEDER/AEI) and PDC2021-121093-I00, the "BCAM Severo Ochoa" accreditation of excellence (SEV-2017-0718); and the Basque Government through the BERC 2018-2021 program, the three Elkartek projects 3KIA (KK-2020/00049), EXPERTIA (KK-2021/00048), and SIGZE (KK-2021/00095), and the Consolidated Research Group MATHMODE (IT1294-19) given by the Department of Education.

References

[1] Farrar C, Worden K. Structural Health Monitoring A Machine Learning Perspective. Wiley; 2013, http://dx.doi.org/10.1002/9781118443118.

[2] Brownjohn JM, de Stefano A, Xu YL, Wenzel H, Aktan AE. Vibration-based monitoring of civil infrastructure: challenges and successes. J Civ Struct Health Monit 2011;1(3-4):79–95. http://dx.doi.org/10.1007/s13349-011-0009-5.

[3] Friswell MI. Damage identification using inverse methods. Phil Trans R Soc A 2007;365(1851):393–410. http://dx.doi.org/10.1098/rsta.2006.1930.

[4] An Y, Chatzi E, Sim S-H, Laflamme S, Blachowski B, Ou J. Recent progress and future trends on damage identification methods for bridge structures. Struct. Control Health Monit 2019;26(10):e2416. http://dx.doi.org/10.1002/stc.2416, arXiv:https://onlinelibrary.wiley.com/doi/pdf/10.1002/stc.2416 e2416 STC-18-0435.R3 https://onlinelibrary.wiley.com/doi/abs/10.1002/stc.2416.

[5] Carden EP, Fanning P. Vibration based condition monitoring: a review. Struct Health Monit 2004;3(4):355–77. http://dx.doi.org/10.1177/1475921704047500.

[6] Alves V, Cury A. A fast and efficient feature extraction methodology for structural damage localization based on raw acceleration measurements. Struct Control Health Monit 2021;28(7):e2748. http://dx.doi.org/10.1002/stc.2748, arXiv:https://onlinelibrary.wiley.com/doi/pdf/10.1002/stc.2748 https://onlinelibrary.wiley.com/doi/abs/10.1002/stc.2748.

[7] Steffen V, Rade DA. Model-based inverse problems in structural dynamics. In: Damage prognosis: For aerospace, civil and mechanical systems. Wiley; 2005, p. 131–75. http://dx.doi.org/10.1002/0470869097.ch7.

[8] Friswell MI, Mottershead JE. Finite element model updating in structural dynamics. Solid Mechanics and its Applications, 38, Dordrecht: Springer Netherlands; 1995, http://dx.doi.org/10.1007/978-94-015-8508-8, http://link.springer.com/10.1007/978-94-015-8508-8.

[9] Liu T, Zhang Q, Zordan T, Briseghella B. Finite element model updating of canonica bridge using experimental modal data and genetic algorithm. Struct Eng Int 2016;26(1):27–36. http://dx.doi.org/10.2749/101686616X14480232444405, https://www.tandfonline.com/doi/full/10.2749/101686616X14480232444405.

[10] Tran-Ngoc H, Khatir S, De Roeck G, Bui-Tien T, Nguyen-Ngoc L, Abdel Wahab M. Model updating for nam O bridge using particle swarm optimization algorithm and genetic algorithm. Sensors 2018;18(12):4131. http://dx.doi.org/10.3390/s18124131, http://www.mdpi.com/1424-8220/18/12/4131.

[11] Alves VN, de Oliveira MM, Ribeiro D, Calçada R, Cury A. Model-based damage identification of railway bridges using genetic algorithms. Eng Fail Anal 2020;118:104845. http://dx.doi.org/10.1016/j.engfailanal.2020.104845, https://www.sciencedirect.com/science/article/pii/S1350630720306580.

[12] Marwala T. Finite element model updating using computational intelligence techniques: applications to structural dynamics. In: Finite-element-model updating using computional intelligence techniques: Applications to structural dynamics. Springer; 2010, http://dx.doi.org/10.1007/978-1-84996-323-7.

[13] Santos JP, Orcesi AD, Crémona C, Silveira P. Baseline-free real-time assessment of structural changes. Struct Infrastruct Eng 2015;11(2):145–61. http://dx.doi.org/10.1080/15732479.2013.858169.

[14] Salehi H, Burgueño R. Emerging artificial intelligence methods in structural engineering. Eng Struct 2018;171(April):170–89. http://dx.doi.org/10.1016/j.engstruct.2018.05.084.

[15] Azimi M, Eslamlou AD, Pekcan G. Data-driven structural health monitoring and damage detection through deep learning: state-of-the-art review. Sensors 2020;20(10):2778. http://dx.doi.org/10.3390/s20102778, https://www.mdpi.com/1424-8220/20/10/2778.

[16] Sun L, Shang Z, Xia Y, Bhowmick S, Nagarajaiah S. Review of bridge structural health monitoring aided by big data and artificial intelligence: from condition assessment to damage detection. J Struct Eng 2020;146:04020073. http://dx.doi.org/10.1061/(ASCE)ST.1943-541X.0002535.

[17] Abdeljaber O, Avci O, Kiranyaz S, Gabbouj M, Inman DJ. Real-time vibration-based structural damage detection using one-dimensional convolutional neural networks. J Sound Vib 2017;388(February):154–70. http://dx.doi.org/10.1016/j.jsv.2016.10.043.

[18] Pathirage CSN, Li J, Li L, Hao H, Liu W, Ni P. Structural damage identification based on autoencoder neural networks and deep learning. Eng Struct 2018;172(January):13–28. http://dx.doi.org/10.1016/j.engstruct.2018.05.109.

[19] Avci O, Abdeljaber O, Kiranyaz S, Hussein M, Gabbouj M, Inman DJ. A review of vibration-based damage detection in civil structures: from traditional methods to machine learning and deep learning applications. Mech Syst Signal Process 2021;147:107077. http://dx.doi.org/10.1016/j.ymssp.2020.107077.

[20] Hou R, Xia Y. Review on the new development of vibration-based damage identification for civil engineering structures: 2010–2019. J Sound Vib 2021;491:115741. http://dx.doi.org/10.1016/j.jsv.2020.115741, https://www.sciencedirect.com/science/article/pii/S0022460X2030571X.

[21] Mujica L, Rodellar J, Guemes A, López-Diez J. Pca based measures: q-statistic and t2-statistic for assessing damages in structures. In: Proceedings of the 4th european workshop on structural health monitoring. 2008, p. 1088–95.

[22] Dervilis N, Antoniadou I, Barthorpe RJ, Cross EJ, Worden K. Robust methods for outlier detection and regression for SHM applications. Int J Sustain Mater Struct Syst 2015;2(1/2):3. http://dx.doi.org/10.1504/ijsmss.2015.078354.

[23] Chalapathy R, Menon AK, Chawla S. Anomaly detection using one-class neural networks. Comput Sci Math 2018;abs/1802.06360. arXiv:1802.06360.

[24] Garcia D, Fernandez-Navamuel A, Sánchez D, Alvear D, Pardo D. Bearing assessment tool for longitudinal bridge performance. J Civ Struct Health Monit 2020;10:1–14. http://dx.doi.org/10.1007/s13349-020-00432-1.

[25] Seventekidis P, Giagopoulos D, Arailopoulos A, Markogiannaki O. Damage identification of structures through machine learning techniques with updated finite element models and experimental validations. In: Model validation and uncertainty quantification, vol. 3. Cham: Springer International Publishing; 2020, p. 143–54.

[26] Zhang Z, Sun C. Structural damage identification via physics-guided machine learning: a methodology integrating pattern recognition with finite element model updating. Struct Health Monit 2021;20(4):1675–88. http://dx.doi.org/10.1177/1475921720927488, arXiv:10.1177/1475921720927488.

[27] Mousavi Z, Ettefagh MM, Sadeghi MH, Razavi SN. Developing deep neural network for damage detection of beam-like structures using dynamic response based on FE model and real healthy state. Appl Acoust 2020;168:107402. http://dx.doi.org/10.1016/j.apacoust.2020.107402, http://www.sciencedirect.com/science/article/pii/S0003682X20305065.

[28] Seventekidis P, Giagopoulos D. A combined finite element and hierarchical deep learning approach for structural health monitoring: test on a pin-joint composite truss structure. Mech Syst Signal Process 2021;157:107735. http://dx.doi.org/10.1016/j.ymssp.2021.107735, https://www.sciencedirect.com/science/article/pii/S0888327021001308.

[29] Seventekidis P, Giagopoulos D, Arailopoulos A, Markogiannaki O. Structural health monitoring using deep learning with optimal finite element model generated data. Mech Syst Signal Process 2020;145:106972. http://dx.doi.org/10.1016/j.ymssp.2020.106972, https://www.sciencedirect.com/science/article/pii/S0888327020303587.

[30] Worden K, Manson G. The application of machine learning to structural health monitoring. Phil Trans R Soc A 2007;365(1851):515–37. http://dx.doi.org/10.1098/rsta.2006.1938, arXiv:https://royalsocietypublishing.org/doi/pdf/10.1098/rsta.2006.1938.

[31] Giagopoulos D, Arailopoulos A, Dertimanis V, Papadimitriou C, Chatzi E, Grompanopoulos K. Structural health monitoring and fatigue damage estimation using vibration measurements and finite element model updating. Struct Health Monit 2019;18(4):1189–206. http://dx.doi.org/10.1177/1475921718790188.

[32] Zakić BD, Ryzynski A, Guo-Hong C, Jokela J. Classification of damage in concrete bridges. Mater Struct 1991;24(4):268–75. http://dx.doi.org/10.1007/BF02472082.

[33] Biondini F, Vergani M. Damage modeling and nonlinear analysis of concrete bridges under corrosion. In: 6th International conference on bridge maintenance, safety and management. 2012, p. 949–57. http://dx.doi.org/10.1201/b12352-132.

[34] Teughels A, Maeck J, De Roeck G. Damage assessment by FE model updating using damage functions. Comput Struct 2002;80(25):1869–79. http://dx.doi.org/10.1016/S0045-7949(02)00217-1.

[35] Simoen E, De Roeck G, Lombaert G. Dealing with uncertainty in model updating for damage assessment: a review. Mech Syst Signal Process 2015;56:123–49. http://dx.doi.org/10.1016/j.ymssp.2014.11.001, http://dx.doi.org/10.1016/j.ymssp.2014.11.001.

[36] Bourlard H, Kamp Y. Auto-association by multilayer perceptrons and singular value decomposition. Biol cybern 1988;59:291–4. http://dx.doi.org/10.1007/BF00332918.

[37] Hinton GE, Salakhutdinov RR. Reducing the dimensionality of data with neural networks. Science 2006;313:504 – 507.

[38] Goodfellow I, Bengio Y, Courville A. Deep learning. The MIT Press; 2016.

[39] Angelov P, Soares E. Towards explainable deep neural networks (xDNN). Neural Netw 2020;130:185–94. http://dx.doi.org/10.1016/j.neunet.2020.07.010, arXiv:1912.02523.

[40] Magalhães F, Cunha A, Caetano E. Vibration based structural health monitoring of an arch bridge: from automated oma to damage detection. Mech Syst Signal Process 2012;28:212–28. http://dx.doi.org/10.1016/j.ymssp.2011.06.011, Interdisciplinary and Integration Aspects in Structural Health Monitoring https://www.sciencedirect.com/science/article/pii/S0888327011002330.

[41] Reynders E, Houbrechts J, De Roeck G. Fully automated (operational) modal analysis. Mech Syst Signal Process 2012;29:228–50. http://dx.doi.org/10.1016/j.ymssp.2012.01.007.

[42] Santos J, Crémona C, Silveira P. Automatic operational modal analysis of complex civil infrastructures. Struct Eng Int 2020;30(3):365–80. http://dx.doi.org/10.1080/10168664.2020.1749012, arXiv:10.1080/10168664.2020.1749012.

[43] Magalhães F, Cunha A. Explaining operational modal analysis with data from an arch bridge. Mech Syst Signal Process 2011;25(5):1431–50. http://dx.doi.org/10.1016/j.ymssp.2010.08.001, https://www.sciencedirect.com/science/article/pii/S0888327010002864.

[44] Giagopoulos D, Arailopoulos A, Dertimanis V, Papadimitriou C, Chatzi E, Grompanopoulos K. Structural health monitoring and fatigue damage estimation using vibration measurements and finite element model updating. Struct Health Monit 2019;18(4):1189–206. http://dx.doi.org/10.1177/1475921718790188.

[45] Shahriari M, Pardo D, Rivera JA, Torres-Verdín C, Picon A, Del Ser J, et al. Error control and loss functions for the deep learning inversion of borehole resistivity measurements. Int J Numer Methods Eng 2021;122(6):1629–57. http://dx.doi.org/10.1002/nme.6593, arXiv:https://onlinelibrary.wiley.com/doi/pdf/10.1002/nme.6593.

[46] Pozo F, Arruga I, Mujica LE, Ruiz M, Podivilova E. Detection of structural changes through principal component analysis and multivariate statistical inference. Struct Health Monit 2016;15(2):127–42. http://dx.doi.org/10.1177/1475921715624504.

[47] Abadi M, Barham P, Chen J, Chen Z, Davis A, Dean J, et al. Tensorflow: a system for large-scale machine learning. 2016, arXiv:1605.08695.

[48] Magalhães F, Cunha Á, Caetano E. Dynamic monitoring of a long span arch bridge. Eng Struct 2008;30(11):3034–44. http://dx.doi.org/10.1016/j.engstruct.2008.04.020.

[49] Zhang G, Moutinho C, Magalhães F. Improved modal identification using wireless continuous dynamic monitoring systems without real time synchronization. Measurement 2021;171:108754. http://dx.doi.org/10.1016/j.measurement.2020.108754, https://www.sciencedirect.com/science/article/pii/S0263224120312549.

[50] Moughty JJ, Casas JR. A state of the art review of modal-based damage detection in bridges: development, challenges, and solutions. Appl Sci (Switzerland) 2017;7(5). http://dx.doi.org/10.3390/app7050510.

[51] Roy K, Ray-Chaudhuri S. Fundamental mode shape and its derivatives in structural damage localization. J Sound Vib 2013;332(21):5584–93. http://dx.doi.org/10.1016/j.jsv.2013.05.003, https://www.sciencedirect.com/science/article/pii/S0022460X13004082.

[52] Kingma DP, Ba JL. Adam: a method for stochastic optimization. In: 3rd international conference on learning representations, ICLR 2015 - conference track proceedings. 2015, p. 1–15, arXiv:1412.6980.

[53] Asuero AG, Sayago A, González AG. The correlation coefficient: an overview. Crit Rev Anal Chem 2006;36(1):41–59. http://dx.doi.org/10.1080/10408340500526766.

[54] Rainieri C, Fabbrocino G. Operational modal analysis of civil engineering structures, an introduction and a guide for applications. 2014, p. 322. http://dx.doi.org/10.1007/978-1-4939-0767-0.

[55] Langone R, Reynders E, Mehrkanoon S, Suykens JA. Automated structural health monitoring based on adaptive kernel spectral clustering. Mech Syst Signal Process 2017;90:64–78. http://dx.doi.org/10.1016/j.ymssp.2016.12.002, https://www.sciencedirect.com/science/article/pii/S0888327016305131.

[56] Reynders E, Teughels A, Roeck GD. Finite element model updating and structural damage identification using omax data. Mech Syst Signal Process 2010;24(5):1306–23. http://dx.doi.org/10.1016/j.ymssp.2010.03.014.

[57] Teughels A, De Roeck G. Structural damage identification of the highway bridge z24 by fe model updating. J Sound Vib 2004;278(3):589–610. http://dx.doi.org/10.1016/j.jsv.2003.10.041.

[58] Kullaa J. Damage detection of the Z24 bridge using control charts. Mech Syst Signal Process 2003;17(1):163–70. http://dx.doi.org/10.1006/mssp.2002.1555.

[59] De Roeck G. The state-of-the-art of damage detection by vibration monitoring: the simces experience. J Struct Control 2003;10(2):127–34. http://dx.doi.org/10.1002/stc.20.

[60] Reynders E, Schevenels M, De roeck G. Macec 3.3. KLEUVEN; 2014, p. 149.

[61] Fritzen C-P. Vibration-based structural health monitoring – concepts and applications. Key Eng Mater - KEY ENG MAT 2005;293. http://dx.doi.org/10.4028/www.scientific.net/KEM.293-294.3.

[62] Garibaldi L, Marchesiello S, Bonisoli E. Identification and up-dating over the z24 benchmark. Mech Syst Signal Process 2003;17(1):153–61. http://dx.doi.org/10.1006/mssp.2002.1553, https://www.sciencedirect.com/science/article/pii/S0888327002915530.

[63] Levin RI, Lieven NA. Dynamic finite element model updating using simulated annealing and genetic algorithms. Mech Syst Signal Process 1998;12(1):91–120. http://dx.doi.org/10.1006/mssp.1996.0136.

[64] Pastor M, Binda M, Harčarik T. Modal assurance criterion. Procedia Eng 2012;48:543–8. http://dx.doi.org/10.1016/j.proeng.2012.09.551.

[65] Brincker R, Andersen P, Zhang L. Modal identification and damage detection on a concrete highway bridge by frequency domain decomposition. Struct Eng World Congr 2002;1–8.

[66] Peeters B, De Roeck G. One-year monitoring of the z24-bridge: environmental effectsversus damage events. Earthq Eng Struct Dyn 2001;30(2):149–71. http://dx.doi.org/10.1002/1096-9845(200102)30:2<149::AID-EQE1>3.0.CO;2-Z.